Clinical Science (2017) **131** 2745–2752
https://doi.org/10.1042/CS20171265

PORTLAND PRESS

Research Article

The perivascular pathways for influx of cerebrospinal fluid are most efficient in the midbrain

Howard Dobson[1,2,3], Matthew MacGregor Sharp[4], Richard Cumpsty[4], Theodore P. Criswell[4], Tyler Wellman[1], Ciara Finucane[1], Jenna M. Sullivan[1], Roy O. Weller[4], Ajay Verma[5] and Roxana O. Carare[4]

[1]inviCRO, Boston, U.S.A.; [2]Department of Clinical Studies, University of Guelph, Ontario, Canada; [3]Department of Biomedical Physics, Western University; [4]Faculty of Medicine, Institute for Life Sciences, Southampton General Hospital, University of Southampton, South Academic Block, MP806, Tremona Road, Southampton, Hampshire SO166YD, U.K.; [5]Biogen, U.S.A.

Correspondence: Roxana O. Carare (rcn@soton.ac.uk)

Although there are no conventional lymphatic vessels in the brain, fluid and solutes drain along basement membranes (BMs) of cerebral capillaries and arteries towards the subarachnoid space and cervical lymph nodes. Convective influx/glymphatic entry of the cerebrospinal fluid (CSF) into the brain parenchyma occurs along the pial-glial BMs of arteries. This project tested the hypotheses that pial-glial BM of arteries are thicker in the midbrain, allowing more glymphatic entry of CSF. The *in vivo* MRI and PET images were obtained from a 4.2-year-old dog, whereas the post-mortem electron microscopy was performed in a 12-year-old dog. We demonstrated a significant increase in the thickness of the pial-glial BM in the midbrain compared with the same BM in different regions of the brain and an increase in the convective influx of fluid from the subarachnoid space. These results are highly significant for the intrathecal drug delivery into the brain, indicating that the midbrain is better equipped for convective influx/glymphatic entry of the CSF.

Introduction

It has been known for over 30 years that tracer injected into the cerebrospinal fluid (CSF) of the cisterna magna of rats passed into the surface of the brain along the outer aspects of arteries, as convective influx [1]. Using modern imaging techniques such as multiphoton microscopy in mice that overexpress green fluorescent protein under the endothelium-specific Tie2 promoter as well as NG2-DsRed mice expressing the red fluorescent protein DsRed under the control of the NG2 promoter, Iliff et al. have revisited the physiology of convective influx and have demonstrated that it depends upon the Aquaporin 4 expression on astrocyte end feet [2]. The process was renamed glymphatic or paravascular entry of solutes into the cerebral parenchyma [2]. It was demonstrated that tracers injected into the CSF reach the level of capillaries in the brain within 30 min of their injection into the cisterna magna, but the exact route taken was uncertain. Recently our group has shown that convective influx/glymphatic communication of CSF with the cerebral parenchyma allows penetration of nanoparticles of 20 nm into the parenchyma, along the pial-glial basement membranes (BM), but this occurs only at distances of approximately 100 μm from the meningeal surface of the brain and the nanoparticles remain within pial-glial BM, without diffusion into the parenchyma [3].

In the present study we tested the hypothesis that pial-glial BM are thicker in the regions of enhanced glymphatic flow of CSF into the brain. To test this hypothesis we performed a detailed analysis using *in vivo* imaging with contrast enhanced MRI with Gd-DTPA injected into the CSF of an aged dog, followed by a detailed study of the pial-glial compartment by electron microscopy.

Received: 04 August 2017
Revised: 07 October 2017
Accepted: 09 October 2017

Accepted Manuscript Online: 11 October 2017
Version of Record published: 13 November 2017

Clinical Science (2017) **131** 2745–2752
https://doi.org/10.1042/CS20171265

Experimental procedures

In vivo procedures

A 4.2-year-old Beagle dog was enrolled in the study. Anaesthesia was induced with propofol (7 mg/kg) followed by endotracheal intubation. Anaesthesia was maintained with isoflurane (1.5–2%) in oxygen with mechanical ventilation. Normal physiology was maintained under anaesthesia by monitoring heart rate, respiratory rate, systolic, diastolic and mean blood pressure, blood oxygen saturation and end tidal CO^2. The concentration of isoflurane was adjusted as necessary to maintain normal physiological conditions. A tapered 3–6F polyurethane catheter with a rounded tip and side ports (ITC-05, SAI infusion Technologies, Lake Villa, IL, U.S.A.) was surgically implanted with the tip in the subarachnoid space at the cisterna magna. The dog was then transferred to an integrated 3T MRI/PET unit. Baseline T1 weighted MR images were acquired.

A mixture of gadopentetate dimeglumine (Magnevist, Bayer PLC, Mississauga, ONT, Canada) diluted to 0.125 mM with sterile water and 23.2 MBq Zr^{89}-DTPA (Prepared by 3D Imaging, Maumelle, AR, U.S.A.) was infused at a rate of 10 μL/m over 50 min. Starting at the beginning of infusion repeated T1 weighted MR images were collected along with a PET image acquisition. The PET data were attenuation corrected based on MR determined attenuation corrections. Each MR image required 5 min to acquire and the PET data were post processed into 5 min bins. On completion of the imaging the catheter was removed and the dog recovered from anaesthesia.

The present study was conducted in full compliance with the inviCRO Institutional Animal Care and Use Committee (IACUC) policies and procedures, which follow the recommendations of The Guide for the Care and Use of Laboratory Animals (The Guide, Institute of Laboratory Animal Resources, National Academy Press, Washington, D.C., 8th Edition, 2011). Veterinary medicine for all research animals is provided by a board-certified veterinarian (Howard Dobson), who also serves as a council member for the Association for Assessment and Accreditation of Laboratory Animal Care International (AAALAC International).

Image analysis

The brain images were segmented using a 45 region canine brain atlas (Proprietary canine 45 region brain atlas inviCRO LLC, Boston, MA, U.S.A.). For each region time activity curves were developed for both the gadopentetate dimeglumine and Zr^{89}-DTPA. Videos of the changes in distribution of the contrast agents over time were also reviewed to qualitatively assess the temporal changes.

Ex vivo samples

Using the same anaesthetic regime described above, a 12-year-old Beagle dog was perfused intracardially with 0.1 M piperazine-*N*,*N*′-bis(2-ethanesulfonic acid) buffer (PIPES, pH 7.2) followed by 4% formaldehyde plus 3% glutaraldehyde in 0.1 M PIPES buffer at pH 7.2. As for the *in vivo* work, the present study was carried out at a facility licensed under the Ontario Animals for Research Act and accredited with the Canadian Council on Animal Care, conducted in full compliance with the inviCRO Institutional Animal Care and Use Committee (IACUC) policies and procedures and approved by the local Animal Care Committee.

The brain was removed, post fixed overnight in fresh fixative and then sectioned into 10 mm corronal slices in preparation for a quantitative and qualitative study of the arterial pial-glial compartment by transmission electron microscopy (TEM). Arteries were distinguished from veins according to the ratio between the areas of the lumen and vessel wall. We first established using the presence of complete rings of smooth muscle cells in the walls of vessels as an indicator of arteries that for arteries, the area of lumen is on average 0.59 × smaller than area of vessel wall. For veins, the area of the lumen is on average 2.42 × larger than the area of the wall. Pial sheaths were identified by the presence of desmosomes [4].

All tissue was processed for electron microscopy following a protocol developed within the Biomedical Imaging Unit, University of Southampton [5] and with approval from research and innovation services nr 13575/58.

Electron microscopy

Regions of midbrain, cerebellum, thalamus, hypothalamus, periventricular white matter (PVWM) and cortex were microdisected from 10 mm corronal slices and processed for TEM. Three arteries from each region were assessed for differences in the pial-glial compartment by comparing pial-glial, smooth muscle and endothelial BM thickness from three randomly chosen locations. iTEM software (Universal TEM Imaging platform, Soft Imaging System, Münster, Germany) was used to take 10 measurements of the width of each BM. To reduce artefactual bias (e.g. from plane of section) the thickness of the pial-glial or smooth muscle BM was divided by the thickness of the endothelial BM to create a ratio. These ratios were then analysed for statistical differences.

Statistical analysis

Descriptive statistics (mean and standard deviation) were presented for the dependent variable pial-glial or smooth muscle BM thickness/endothelial BM thickness ratio in each of the six brain regions analysed, as well as in the pial-glial and smooth muscle BM. A linear regression model was used to compare the ratio between the six regions in either the pial-glial or smooth muscle BM adjusted for arteries and locations. Bonferroni correction was applied to adjust for the multiple comparisons between regions. Another linear regression model was applied to compare the calculated ratio between the pial-glial or smooth muscle BM in each of the six regions, which was similarly adjusted for arteries and locations. Bonferroni correction was also applied to adjust for the multiple comparisons between BMs. Mean difference of the ratio between regions and between BMs along with 95% confidence interval and *P* value were presented. Statistical significance was set at 5%. All statistical analyses were performed using SPSS version 22.

Results

Enhanced glymphatic/convective influx of tracer in the midbrain

In vivo imaging using PET and Zr^{89}-DTPA revealed that at 50 min after infusion into the CSF, there was an area of high intensity of tracer within the midbrain. This area progressively declined in intensity at 100, 150 and 200 min post administration of Zr^{89}-DTPA (Figure 1 , Figure 2).

Arteries in the midbrain have an enlarged pial-glial compartment

Arteries from the midbrain, cerebellum, thalamus, hypothalamus, PVWM and cortex were assessed for differences in the pial-glial compartment by comparing pial-glial, smooth muscle and endothelial BM thickness by TEM. The pial-glial BM of arteries in the midbrain were found to be at least three times the thickness of any other cerebrovascular BM analysed. PVWM arteries showed a significantly higher smooth muscle BM/endothelial BM ratio compared with the same ratio in the cortex or the thalamus (Figure 3, Table 1). The BMs surrounding the smooth muscle cells of arteries in the hippocampus are thicker compared with the thalamus and compared with the cortex (Table 1).

Discussion

The present study has demonstrated that tracers entering the surface of the brain from the CSF by the convective influx/glymphatic system penetrate more deeply into the midbrain than in any other region of a 4.2-year-old dog brain. Entry of fluid and tracers from the CSF into the surface of the brain is along the pial-glial BMs on the outer aspects of arteries. Enhanced penetration of tracers into the midbrain is correlated, in the present study, with the greater thickness of pial-glial BMs around arteries in the midbrain than in other regions of the brain. In addition, the present study has shown that tracers entering the brain from the CSF persist in a diffuse distribution within the brain for at least 200 min. A previous study in three *Macaca facicularis* primates demonstrated that the tracer Gadolinium chelate (DOTA-Gd) entered the superficial layers of the midbrain and cerebral cortex from the CSF within 20 min of intrathecal infusion [6]. These combined studies indicate that tracers entering the brain from the CSF may persist within the CNS parenchyma for at least 2 h.

The capacity of the subarachnoid spaces over the cerebral cortex and midbrain are much closer in dogs than in rodents, in relation to humans. The main reason for using the dog as an experimental model is that the ultrastructural features of the perivascular compartments in the cerebral cortex of the dog are very similar to those shown in the literature in humans. One of the other major differences between quadrupeds and bipeds is the size of the arachnoid villi and granulations. These are very small in quadrupeds such as rats and sheep and much more substantial in primates including humans. However, we do emphasise that the CSF transport in the present study is visualised in the setting of alternating positive/negative intracranial pressure (in the setting of mechanical ventilation) and it is possible that this transport pattern would not occur with spontaneous ventilation and normal negative thoracic pressures.

The brainstem has been identified as an area of high contrast enhancement of CSF after intrathecal gadobutrol administration in a young female [7] and methodology is constantly improving for the assessment of glymphatic flow in human brains [8]. Previous research demonstrates that the pial-glial BMs are the entry routes for CSF into the brain [9]. As tracers reach capillary level, they are likely diffusing through the extracellular spaces of the brain where they are likely taken up by cells and a part of the tracer will be returning towards the surface of the brain through the intramural periarterial drainage pathways for the interstitial fluid (ISF).

The data derived from the present study support the concept that the intrathecal route has potential for drug delivery particularly to the midbrain. While such delivery may not feasible for deeper structures in the cerebral hemispheres, recent trials conducted by Biogen for treatment of spinal muscular atrophy in children have yielded successful

Clinical Science (2017) **131** 2745–2752
https://doi.org/10.1042/CS20171265

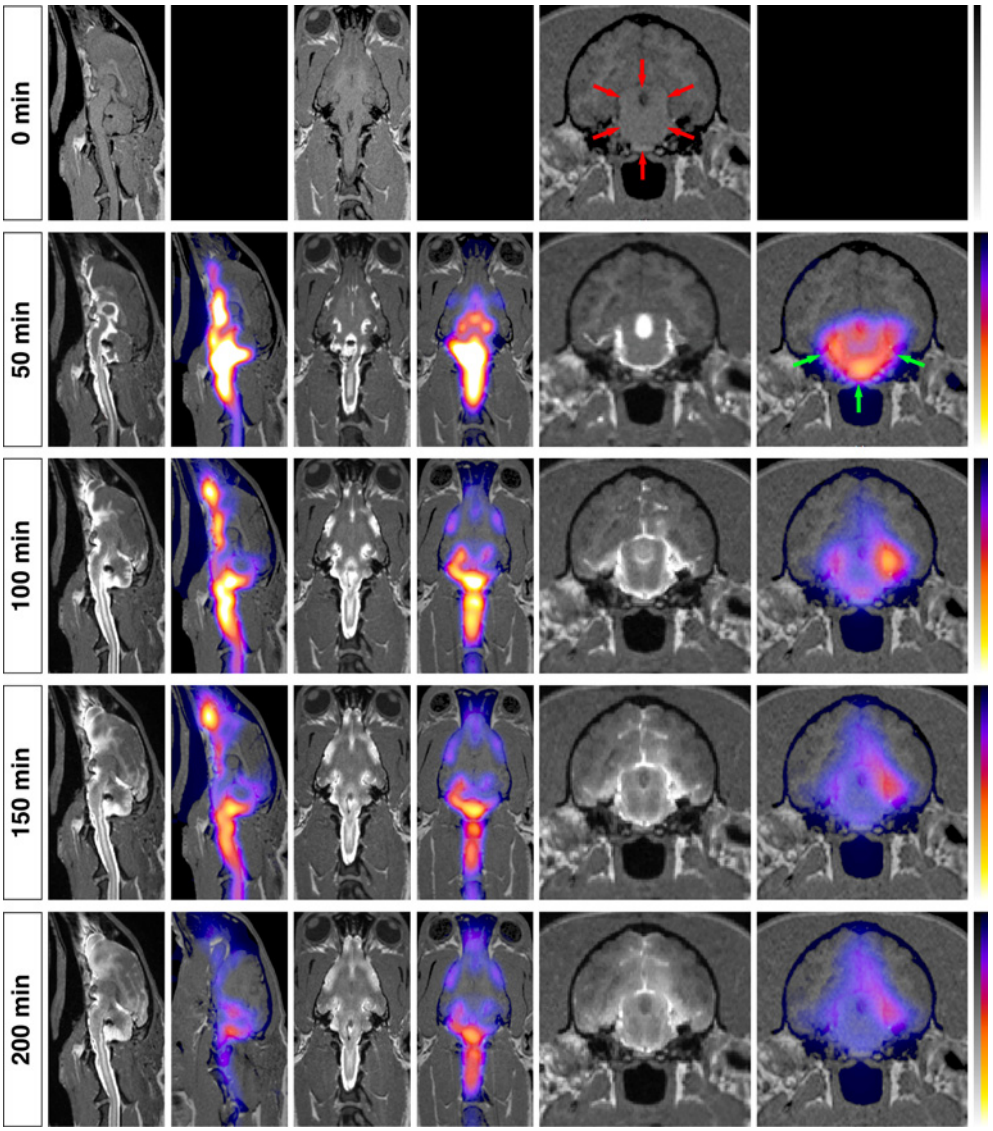

Figure 1. A series of orthogonal images MR images (first, third and fifth columns) with PET images overlain (second, fourth and sixth columns)

The top row are pre-administration of gadopentetate dimeglumine and Zr89-DTPA. The lower rows are at 50, 100, 150 and 200 min post-administration, respectively. The red arrows indicate the region of the midbrain and the green arrows point to a U-shaped area of greater intensity of the radioactivity in the subarachnoid space which can also be identified as high signal intensity in the corresponding MR image in column five. The images demonstrate the rapid accumulation of the ^{89}Zr-DTPA in the midbrain.

outcomes [10-14]. The successful results of these trials suggest that antisense oligonucleotides enter the brain preferentially along the pial-glial BMs of arterioles in the midbrain, as demonstrated in the present study. Recent advances in imaging show the possibility of visualising individual nuclei in the brainstem from which dopaminergic, serotonergic and noradrenergic innervations arise; this suggests that the action of drug therapies administered by intrathecal injection could be monitored by such imaging techniques [15,16].

Vascular BMs surrounding CNS capillaries and arteries play key roles in the bulk transport of fluids and solutes within the CNS [3]. In most organs, homoeostasis of the extracellular environment is maintained by the supply of nutrients from the blood and by the elimination of fluid and solutes along well-defined lymphatic vessels. There are no lymphatic vessels in the CNS parenchyma, so BMs around arteries and capillaries are the major routes by which CSF enters the CNS and are also the major routes by which fluid and solutes leave the CNS and drain to lymph nodes. However, the route of entry of CSF into the brain by the pial-glial BMs on the outside of arteries is distinctly separate

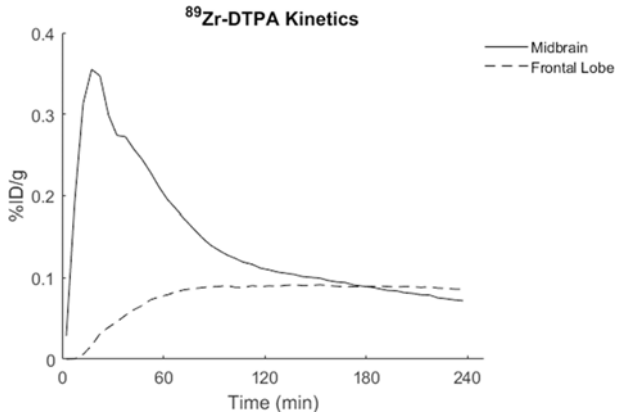

Figure 2. A time activity curve of the midbrain and frontal lobe

Within the first 20 min there was higher concentration of ^{89}Zr-DTPA in the midbrain compared with the frontal lobe.

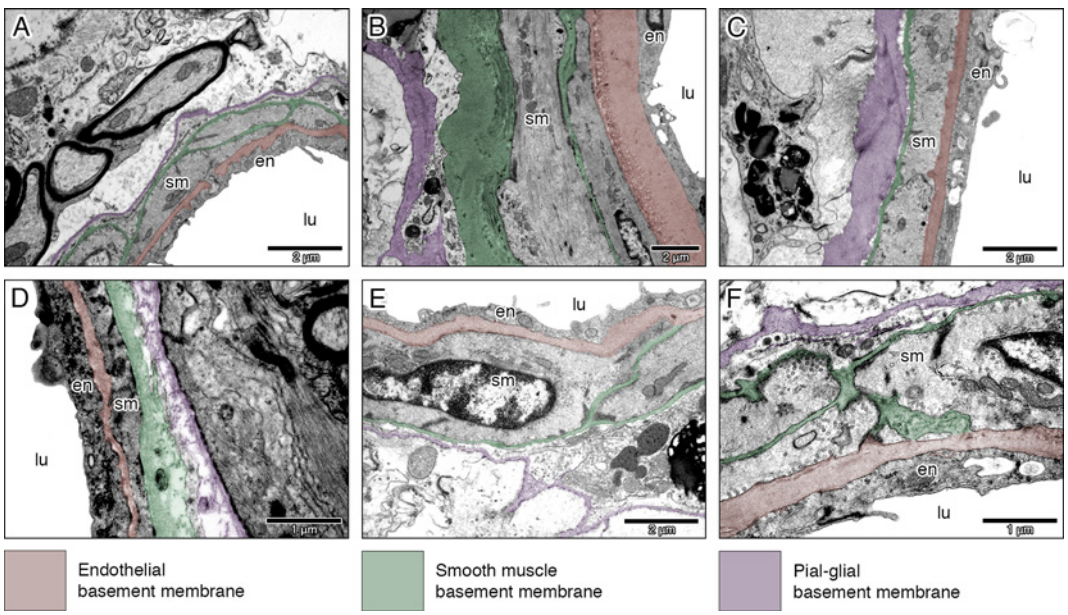

Figure 3. Transmission electron micrographs

Electron micrographs showing regional differences in basement membrane thickness: (A) between arteries in the cerebellum, (B) hippocampus, (C) midbrain, (D) periventricular white matter, (E) thalamus and (F) cortex. The pial-glial BM of arteries in the midbrain were found to be at least three times the thickness of any other cerebrovascular BM analysed. Abbreviation: lumen (lu); endothelium (en) and smooth muscle (sm).

from the intramural perivascular route by which fluid and solutes leave the brain. Fluid and soluble tracers entering the brain along pial-glial BMs on the outer aspects of penetrating arterioles mix with ISF within the brain parenchyma [3]. Such mixing of CSF and ISF appears to be controlled by aquaporin 4 in perivascular astrocyte processes [2]. ISF in the brain is thus a combination of solutes derived from the blood, from tissue metabolism and from the entry of CSF [17]. Tracer studies show that ISF drains rapidly from the brain parenchyma by a continuous pathway starting in the glial-endothelial BMs in the walls of cerebral capillaries and then progressing along BMs that surround smooth muscle cells in the tunica media of cerebral arterioles [18]. At the surface of the brain, the ISF drainage route continues along smooth muscle cell BM in the walls of leptomeningeal arteries eventually to cervical lymph nodes [18]. Thus, lymphatic drainage of the brain parenchyma is along *intramural periarterial drainage* pathways that are almost completely separate from the glymphatic route of entry of CSF into the brain.

Evidence for the intramural periarterial drainage pathway is derived from experimental studies in mice, using soluble tracers, and from the observed accumulation of amyloid beta (Aβ) in this pathway in the walls of arteries as

Clinical Science (2017) **131** 2745–2752
https://doi.org/10.1042/CS20171265

Table 1 The mean thickness of endothelial, smooth muscle and pial-glial BMs expressed as a ratio with the endothelial BMs

Basement membrane	Region	Mean difference*	95% CI*	*P* value
	Midbrain – cortex	6.9141	(6.1779, 7.6503}	<0.001
	Midbrain – cerebellum	6.5709	(5.8118, 7.3299)	<0.001
	Midbrain – PVWM	6.6721	(5.9131, 7.4312}	<0.001
	Midbrain – thalamus	7.0211	(6.2621, 7.7802}	<0.001
	Midbrain – hippocampus	7.0476	(6.2886, 7.8066}	O.001
	Cerebellum – cortex	0.3432	(−0.3930, 1.0794)	1
	Cerebellum – PVWM	0.1013	(−0.6349, 0.8375)	1
Pial-glial	Cerebellum – thalamus	0.4503	(−0.2859, 1.1865)	1
	Cerebellum – hippocampus	0.4768	(−0.2594, 1.2130)	0.851
	PVWM – cortex	0.242	(−0.4942, 0.9782)	1
	PVWM – thalamus	0.349	(−0.3872, 1.0852)	1
	PVWM – hippocampus	0.3755	(−0.3607, 1.1117)	1
	Thalamus – cortex	−0.107	(−0.8432, 0.6292)	1
	Thalamus – hippocampus	0.0265	(−0.7097, 0.7627)	1
	Hippocampus – cortex	−0.1335	(−0.8697, 0.6027)	1
	Midbrain – cortex	0.5405	(0.3129, 0.7680}	<0.001
	Midbrain – cerebellum	0.4302	(0.2083, 0.6521}	<0.001
	Midbrain – PVWM	0.0113	(−0.2105, 0.2332)	1
	Midbrain – thalamus	0.6299	(0.4080, 0.8518}	<0.001
	Midbrain – hippocampus	−0.0587	(−0.2805, 0.1632)	1
	Cerebellum – cortex	0.1103	(−0.1173, 0.3378)	1
	Cerebellum – PVWM	−0.4189	(−0.6464, −0.1913}	<0.001
Smooth muscle	Cerebellum – thalamus	0.1997	(−0.0278, 0.4273)	0.149
	Cerebellum – hippocampus	−0.4889	(−0.7164, −0.2613)	O.001
	PVWM – cortex	0.5291	(0.3016, 0.7567)	O.001
	PVWM – thalamus	0.6186	(0.3910, 0.8461)	0.001
	PVWM – hippocampus	−0.07	(−0.2976, 0.1576)	1
	Thalamus – cortex	−0.0894	(−0.3170, 0.1381)	1
	Thalamus – hippocampus	−0.6886	(−0.9161, −0.4610)	<0.001
	Hippocampus – cortex	0.5991	(0.3716, 0.8267)	<0.001

As there were more than one variable, a linear regression model was applied. The ratios of the thickness of BM were analysed from 10 different locations, in 3 different arteries, in pial-glial, smooth muscle and endothelial BM, in the cerebellum, midbrain, cortex, PVWM, thalamus and hippocampus. As there were multiple comparisons, Bonferroni correction was applied.
*Ratio to endothelial BM (endothelial BM = 1).

cerebral amyloid angiopathy (CAA) in older humans and in Alzheimer's disease [19]. Age is a major risk factor for Alzheimer's disease that is characterised by the accumulation of extracellular Aβ plaques, CAA and the accumulation of intraneuronal hyperphosphorylated tau. Experimental studies have shown that the efficiency of intramural periarterial drainage of Aβ declines with age and this correlates stiffening of arteries and thickening of the smooth muscle cell BMs that form the drainage pathway [20,21].

Thickening of intramural arteriolar BMs with age is not uniform throughout the brain. Smooth muscle cell BMs in the walls of arterioles supplying the cerebral cortex in aged individuals are thicker compared with those in arteries in the thalamus. In rodents, the thickness of capillary BMs in the cerebral cortex, hippocampus and thalamus increase with age but this does not occur in the striatum. Furthermore, the composition of intramural arteriolar BMs in the rodent cortex changes with age showing an increase in the ratio of the pro-amyloidogenic protein perlecan to collagen IV. The age-related chemical changes and increase in thickness of smooth muscle cell BMs in cortical arteries compared with those in the striatum correlates with the far greater load of amyloid plaques and CAA in the cortex in Alzheimer's disease compared with the striatum. This suggests that age-related failure of drainage of Aβ from the brain is related to age-related changes in the walls of arteries and smooth muscle cell BMs.

The results of the present study, those of previous experiments and observations on ageing arteries suggest that there is an interrelationship between the thickness of periarterial BMs and the efficiency of flow of fluid and tracers along the BMs. However, there is a paradox that requires further investigation. The pial-glial BMs on the outer aspects of arteries are thicker in the midbrain of the dog and this correlates with deeper penetration of CSF tracers into the midbrain

when compared with other areas of the brain. On the other hand, thickening of the intramural smooth muscle cell BMs that form the pathway for drainage of ISF and solutes out of the brain appears to reduce the efficiency of this drainage pathway and this may facilitate the deposition of Aβ in CAA. Despite the paradox, these results emphasise the key role played by perivascular BMs in the transport of fluid and solutes into the brain from the CSF and out of the brain to lymph nodes. The paradox may reflect fundamental differences in the functional properties of the glymphatic versus the intramural periarterial drainage pathways. The physiological characteristics of the CSF-related glymphatic pathways have implications for intrathecal therapies whereas age- related changes in intramural BMs of cerebral arteries appear to play an important role in the aetiology of CAA and Alzheimer's disease.

Clinical perspectives

- The study was undertaken to demonstrate the ultrastructure and regional efficiency for the pathways of convective influx of CSF into the brain.
- Our results using a large mammalian brain (dog) demonstrate that (a) the CSF penetration into the parenchyma is most optimal in the midbrain and (b) the pial-glial BMs that form the pathways for perivascular convective influx of CSF into the parenchyma are thickest in the midbrain compared with other cerebral regions.
- The significance of the results is for intrathecal drug delivery to the brain, suggesting that the midbrain can be easily reached by drugs injected into the CSF.

Ethical statement

All *in vivo* animal procedures were approved by the local Animal Care Committee and the work was carried out at a facility licensed under the Ontario Animals for Research Act and accredited with the Canadian Council on Animal Care.

Funding

This work was supported by the Biogen [Grant No. BI-2014-CR134].

Author Contribution

A.V. and R.O.C. designed the study and selected appropriate methodology. H.D. is the veterinary surgeon who ensured that the dog was devoid of any diseases and performed the *in vivo* imaging, assisted by T.W. and J.M.S. T.P.C. and M.Mc.S. performed the electron microscopy and analyses. C.F. coordinated the work between the different sites and management of all approvals for ethics and transportation of tissue. R.O.W. provided expertise for the interpretation of data. All authors contributed to the manuscript.

Competing Interests

The authors declare that there are no competing interests associated with the manuscript.

Abbreviations

Aβ, amyloid beta; BM, basement membranes; CAA, cerebral amyloid angiopathy; CSF, cerebrospinal fluid; ISF, interstitial fluid; PIPES, piperazine-*N*,*N*′-bis(2-ethanesulfonic acid); PVWM, periventricular white matter; TEM, transmission electron microscopy.

References

1 Rennels, M.L., Gregory, T.F., Blaumanis, O.R., Fujimoto, K. and Grady, P.A. (1985) Evidence for a 'paravascular' fluid circulation in the mammalian central nervous system, provided by the rapid distribution of tracer protein throughout the brain from the subarachnoid space. *Brain Res.* **326**, 47–63
2 Iliff, J.J., Wang, M., Liao, Y., Plogg, B.A., Peng, W., Gundersen, G.A. et al. (2012) A paravascular pathway facilitates CSF flow through the brain parenchyma and the clearance of interstitial solutes, including amyloid beta. *Sci. Transl. Med.* **4**, 147ra11
3 Morris, A.W., Sharp, M.M., Albargothy, N.J., Fernandes, R., Hawkes, C.A., Verma, A. et al. (2016) Vascular basement membranes as pathways for the passage of fluid into and out of the brain. *Acta Neuropathol. (Berl.)* **131**, 725–736
4 Weller, R.O. (2005) Microscopic morphology and histology of the human meninges. *Morphologie* **89**, 22–34

Clinical Science (2017) **131** 2745–2752
https://doi.org/10.1042/CS20171265

5 Siskova, Z., Page, A., O'Connor, V. and Perry, V.H. (2009) Degenerating synaptic boutons in prion disease: microglia activation without synaptic stripping. *Am. J. Pathol.* **175**, 1610–1621
6 Goulay, R., Flament, J., Gauberti, M., Naveau, M., Pasquet, N., Gakuba, C. et al. (2017) Subarachnoid hemorrhage severely impairs brain parenchymal cerebrospinal fluid circulation in nonhuman primate. *Stroke* **48**, 2301–2305
7 Eide, P.K. and Ringstad, G. (2015) MRI with intrathecal MRI gadolinium contrast medium administration: a possible method to assess glymphatic function in human brain. *Acta Radiol. Open* **4**, 2058460115609635
8 Myllyla, T., Harju, M., Korhonen, V., Bykov, A., Kiviniemi, V. and Meglinski, I. (2017) Assessment of the dynamics of human glymphatic system by near-infrared spectroscopy (NIRS). *J. Biophotonics*
9 Morris, A.W., Sharp, M.M., Albargothy, N.J., Fernandes, R., Hawkes, C.A., Verma, A. et al. (2016) Vascular basement membranes as pathways for the passage of fluid into and out of the brain. *Acta Neuropathol. (Berl.)*
10 Bishop, K.M. (2016) Progress and promise of antisense oligonucleotide therapeutics for central nervous system diseases. *Neuropharmacology*
11 Chiriboga, C.A., Swoboda, K.J., Darras, B.T., Iannaccone, S.T., Montes, J., De Vivo, D.C. et al. (2016) Results from a phase 1 study of nusinersen (ISIS-SMN(Rx)) in children with spinal muscular atrophy. *Neurology* **86**, 890–897
12 Finkel, R.S., Chiriboga, C.A., Vajsar, J., Day, J.W., Montes, J., De Vivo, D.C. et al. (2016) Treatment of infantile-onset spinal muscular atrophy with nusinersen: a phase 2, open-label, dose-escalation study. *Lancet* **388**, 3017–3026
13 Hache, M., Swoboda, K.J., Sethna, N., Farrow-Gillespie, A., Khandji, A., Xia, S. et al. (2016) Intrathecal injections in children with spinal muscular atrophy: nusinersen clinical trial experience. *J. Child Neurol.* **31**, 899–906
14 Finkel, R.S., Bishop, K.M. and Nelson, R.M. (2017) Spinal muscular atrophy type I: is it ethical to standardize supportive care intervention in clinical trials? *J. Child Neurol.* **32**, 155–160
15 Sclocco, R., Beissner, F., Bianciardi, M., Polimeni, J.R. and Napadow, V. (2017) Challenges and opportunities for brainstem neuroimaging with ultrahigh field MRI. *Neuroimage* **S1053-8119** (17), 30163–30165
16 Ito, H., Kawaguchi, H., Kodaka, F., Takuwa, H., Ikoma, Y., Shimada, H. et al. (2017) Normative data of dopaminergic neurotransmission functions in substantia nigra measured with MRI and PET: neuromelanin, dopamine synthesis, dopamine transporters, and dopamine D2 receptors. *Neuroimage* **158**, 12–17
17 Abbott, N.J. (2004) Evidence for bulk flow of brain interstitial fluid: significance for physiology and pathology 1. *Neurochem. Int.* **45**, 545–552
18 Carare, R.O., Bernardes-Silva, M., Newman, T.A., Page, A.M., Nicoll, J.A., Perry, V.H. et al. (2008) Solutes, but not cells, drain from the brain parenchyma along basement membranes of capillaries and arteries: significance for cerebral amyloid angiopathy and neuroimmunology. *Neuropathol. Appl. Neurobiol.* **34**, 131–144
19 Carare, R.O., Hawkes, C.A., Jeffrey, M., Kalaria, R.N. and Weller, R.O. (2013) Review: cerebral amyloid angiopathy, prion angiopathy, CADASIL and the spectrum of protein elimination failure angiopathies (PEFA) in neurodegenerative disease with a focus on therapy. *Neuropathol. Appl. Neurobiol.* **39**, 593–611
20 Hawkes, C.A., Hartig, W., Kacza, J., Schliebs, R., Weller, R.O., Nicoll, J.A. et al. (2011) Perivascular drainage of solutes is impaired in the ageing mouse brain and in the presence of cerebral amyloid angiopathy. *Acta. Neuropathol. (Berl.)* **121**, 431–443
21 Hawkes, C.A., Gatherer, M., Sharp, M.M., Dorr, A., Yuen, H.M., Kalaria, R. et al. (2013) Regional differences in the morphological and functional effects of aging on cerebral basement membranes and perivascular drainage of amyloid-beta from the mouse brain. *Aging Cell* **12**, 224–236